

J. Q. Hu

Applied Mechanics Laboratory,
School of Aerospace,
Tsinghua University,
Beijing 100084, China

Z. L. Liu¹

Applied Mechanics Laboratory,
School of Aerospace,
Tsinghua University,
Beijing 100084, China
e-mail: liuzhanli@tsinghua.edu.cn

Y. N. Cui

Applied Mechanics Laboratory,
School of Aerospace,
Tsinghua University,
Beijing 100084, China

Z. J. Wang

Center for Advancing Materials Performance
from the Nanoscale (CAMP-Nano)
& Hysitron Applied
Research Center in China (HARCC),
State Key Laboratory for
Mechanical Behavior of Materials,
Xi'an Jiaotong University,
Xi'an 710049, China

Z. W. Shan

Center for Advancing Materials Performance
from the Nanoscale (CAMP-Nano)
& Hysitron Applied
Research Center in China (HARCC),
State Key Laboratory for
Mechanical Behavior of Materials,
Xi'an Jiaotong University,
Xi'an 710049, China

Z. Zhuang¹

Applied Mechanics Laboratory,
School of Aerospace,
Tsinghua University,
Beijing 100084, China
e-mail: zhuangz@tsinghua.edu.cn

Sensitive Material Behavior: Theoretical Model and Experiment for Compression Collapse of Gold Particles at Submicron Scale

Recent in situ TEM experiments observed that single crystalline gold particles with diameter ranging from 300 to 700 nm suddenly collapse, accompanying numerous dislocations escaping from the free surface during a flat punch pushing toward the particle. This collapse is catastrophic for the microdevices in service. In this work, we numerically and theoretically analyze the collapse mechanisms of this kind of "sensitive material." First, by carrying out molecular dynamics (MD) simulations and finite element (FEM) analysis, we conclude that the strong strain burst in the collapse is derived from the robust emissions of plentiful pile-up dislocations in a particular area. Then, on the basis of numerical analyses, a theoretical model based on the virtual work principle is developed to predict the load–displacement curve during the indentation and reveal the energy dissipation and transformation before the particle collapse. Furthermore, a micromechanics-based dislocation pile-up model is established to quantitatively interpret the mechanism of particle collapse. Based on these studies, we propose the dislocation avalanche at the microscale depends not only on the peak stress but also on the stress gradients. The research is helpful for the design of reliable microdevices. [DOI: 10.1115/1.4027916]

Keywords: sensitive material, single crystal gold particle, compression collapse, theoretic model, submicron scale

1 Introduction

With the rapid development of microelectromechanical systems and the other small-scale devices, submicron materials have recently attracted considerable interests. Recent in situ TEM tests show that plastic behaviors in submicron single crystals such as micropillars or particles differ significantly from macroscopic plastic flow. Besides the well-known size dependent yield strength [1–4], it has also become clear that the plastic deformation at microscale proceeds in the intermittent way, accompanying a strong displacement or strain burst [5–8]. The fine slip bands or lines were widely observed during the strain burst in the single crystalline micropillar compression tests of Cu and Mo [9,10]. Suresh et al. [11] also observed the abrupt displacement burst in

nano-indentation for the metallic material of copper thin films, and similar phenomenon was also discovered in aluminum thin films [12]. Uchic et al. [13] carried out a series of tests on Ni micropillars and revealed that the localized deformation during strain burst is due to the escape of dislocations from free surface. Nix et al. [14] found that the gold pillars may become dislocation starved after each strain burst during the compression. More recently, strain bursts are also discovered in the microshear deformation of gold single crystals, which is ascribed to either the formation of new shear bands or the sudden shear strain accumulation events in existing shear bands [5]. These widely observed "microscale plasticity instability" phenomena in various materials with different shapes bring troubles to control the plastic forming of the microdevices and make it difficult to predict the reliability of microdevice in service.

Motivated by these experimental observations, a lot of theoretical and numerical studies have been carried out to reveal the mechanism of plasticity instability at microscale. Several postulations have been proposed to explain the instability in the bulk

¹Corresponding authors.

Contributed by the Applied Mechanics Division of ASME for publication in the JOURNAL OF APPLIED MECHANICS. Manuscript received May 14, 2014; final manuscript received June 23, 2014; accepted manuscript posted June 27, 2014; published online July 3, 2014. Editor: Yonggang Huang.

single crystalline materials. One of them is that the robust emission of dislocation loops under the indenter at a critical load facilitated the strain burst [15,16]. While some researchers regarded that the indenter would trigger an abrupt invasion when a brittle fracture started from the surface because of the presence of a native oxide or some other coatings at the surface [12,17]. For most cases, multiple displacement bursts are observed in the nano-indentation or compression tests and the indentation response between two successive bursts is nearly elastic; thus, the dislocation nucleation and emission process may be the more probable mechanism for the onset of strain burst. Ispánovity colleagues [18] indicated the fast dislocation avalanches played a dominant role in the plastic response and revealed the relationship between plastic strain rate and the distribution of dislocation velocities. Gerberich et al. [19] established an analytical model from the perspective of energy balance to explain the plastic instability for single and multiple dislocation events occurred in nanoparticles indentation, but the details of instability point and the dislocation configuration were not given. In addition to the theoretical analyses, various numerical simulations have also been carried out to investigate the small-scale instability [20–22]. Xu et al. [23] employed MD to simulate the compression process of Al pillars with different orientations and size, and investigated the mechanisms of jerky deformation by analyzing the nucleation of initial dislocations and the compression orientation. Weinberger and Cai [24] studied the evolution of a dislocation network in a gold nanowire at different orientations in torsion by MD simulations and discussed the influence of the stacking fault energy of the material and the diameter of the nanowire on the stability of dislocation. Moreover, Ng and Ngan [25] found that the frequency of the occurrence of sporadic bursts depended on applied stress, creep time, and pillar size by a series of Monte Carlo simulations. Li et al. [26] recently predicted the instability induced by dislocation nucleation during the indentation of crystal through a multi-scale crystal defect dynamics method. By systematically carrying out 3D discrete dislocation dynamic simulations, Cui et al. [27] found the strain burst during the compression of micropillars was directly controlled by the operation and shutdown of the single arm dislocation source. Above all, the understanding for the mechanism of plasticity instability in micropillars or particles is still very limited and remains to be further explored.

Recently, one kind of new collapse behavior was observed in the compression experiment of single crystalline gold particles with diameter ranging from 300 to 700 nm diameters embedded a half in a silicon substrate. The particle suddenly collapsed and numerous dislocations escaped from the free surface during a flat indenter touching the head of particle. Interestingly, the hemisphere-shaped particle would collapse into a truncated cone without warning. This is very like the sensitive material in nature that the plant immediately gets out of the way when it is touched by the object. So, we term this new collapse behavior as sensitive material phenomenon. However, what happened during the collapse and whether there exists a new stability mechanism, which controls the collapse, remain an opening problem.

In this paper, the compression experiment of single crystalline gold particles is illustrated in Sec. 2. In Sec. 3, first with the help of MD simulations and FEM analysis, we investigate the characterization of plastic deformation under the indenter before particle collapse. Then, on the basis of simulation results, a theoretical model based on virtual work principle is developed in Sec. 4 to understand the energy transformation and predict the load–displacement relation before the particle collapse. Furthermore, a dislocation pile-up model is proposed through the analysis of stress distribution along a slip direction to explain the collapse mechanism. It is found that dislocations would pile up in a stress valley area, which is located at some distance away from the contact surface. The collapse is ascribed to the sudden release of pile-up dislocations from the particle surface in a critical state. We infer that the microscale instability depends not only on the peak stress but also on the stress gradients inside the

hemisphere-shaped specimen. Eventually, some conclusions are given in Sec. 5.

2 Experimental Observations

A series of compression experiments are carried out for the single crystalline gold particles with size ranging from 300 to 700 nm diameters embedded a half in a silicon substrate [28]. In the experiments, the single crystal gold particles are fabricated as the following steps, as illustrated in Fig. 1. First, a special silicon wedge substrate is designed (Fig. 1(a)). Second, a thin SiO₂ layer is deposited on the surface of the silicon wedge substrate as shown in Fig. 1(b). Next, thin Au film is deposited on the surface of the thin SiO₂ layer (Fig. 1(c)) like the second step. At last, the thin Au film is transferred to a furnace and then annealed at 1150 °C in air for 1 h followed by furnace cooling down to room temperature. From above process, some pristine perfect gold particles can be obtained with sizes ranging from 300 to 700 nm embedded a half in silicon substrate as shown in Fig. 1(d).

During the compression test, a flat punch under displacement rate control mode was applied on a particle top. When the punch pushed forward to some critical distance, the gold particle collapsed immediately and was deformed as frustum of a cone as shown in Fig. 2. After the cataclysmic collapse, stable plastic flow proceeded during the following compression. The TEM images, corresponding to the displacement bursts shown in the compressive force–displacement curves in Figs. 2(a), 2(c), and 2(e), are also given, respectively, in Figs. 2(b), 2(d), and 2(f). This collapse always happens without anticipatory warning and will bring troubles for the fabrication of devices at submicron scales.

In the experiments, as the happening of cataclysmic displacement collapses, numerous dislocations escape from the surface and a nearly perfect particle is obtained after collapse. This large displacement collapses are always accompanied by an extremely high contact pressure. For the next stable plastic flow stage, the contact pressure is nearly unchanged. From the observations above, it is found that the collapse is a very complicated process which involves a lot of challenging issues in submicron plasticity: dislocation nucleation under the indenter and at free surface, escape of dislocations from the free surface, interactions between loop- and arc-shaped dislocations in a limited space, etc.

Wang et al. [28] preliminarily proposed that two primary factors are responsible for the cataclysmic displacement collapses. The first one is the possibility of emitting the first dislocation

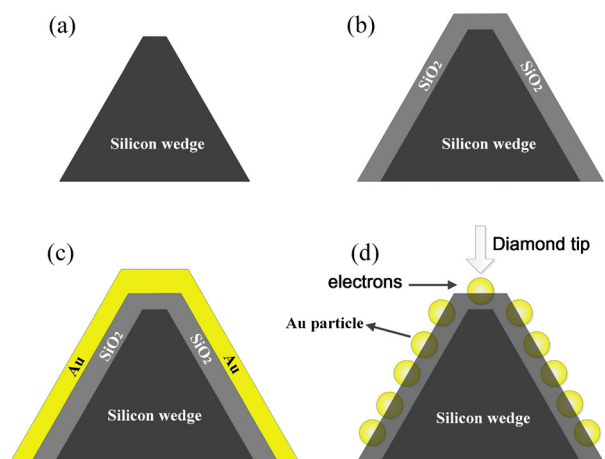


Fig. 1 Process design for compression in situ experiment of gold particle in TEM [28]: (a) silicon wedge substrate; (b) a thin SiO₂ layer is deposited; (c) thin Au film is deposited on the surface of the thin SiO₂ layer; and (d) Au particles are formed after high-temperature annealing and for in situ TEM compression test

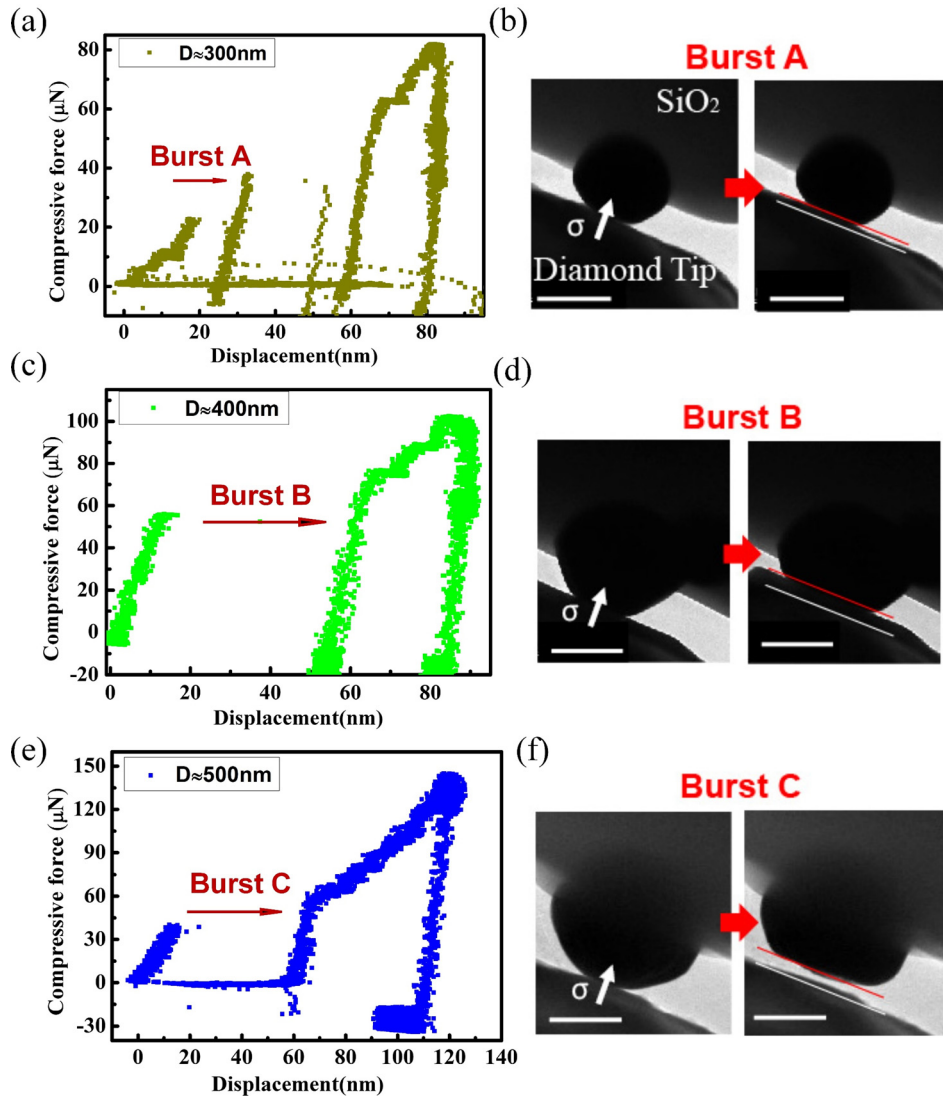


Fig. 2 (a) Compressive force versus displacement of Au particle with diameter 300 nm; (b) TEM images during the burst process; and (c)–(f) experiment data and TEM images for particles with diameter 400 nm and 500 nm, respectively. Experimental data from Wang et al. [28].

from the free surface and the second one is the probability of correlated emissions of hundreds of dislocations. And the first one should be the bottleneck for smaller samples since it is hard to form jammed dislocations or store dislocations inside the samples with small size, so the cataclysmic collapse is due to the very first dislocation nucleation followed by numerous correlated nucleation events under the extremely high stress. While the second one would be dominant for the sample with bigger size, because these internal jammed dislocations could lead to plastic strain and release the high stress close to the indenter, so the displacement collapse would not happen until the storage of jammed dislocations is beyond the samples' capacities.

From the analysis above, it is clear that the strain burst process in small-scale particles is mainly induced by the very first dislocation nucleation event, so the collapse pressure is simply decided by the dislocation nucleation stress. However, for sample with big size, how the dislocations would nucleate and accumulate inside the particles and what happened during the collapse remain unclear. Aiming at studying these issues, both FEM analysis and MD simulation are carried out in Sec. 3 to investigate the details, e.g., the stress distribution and dislocation structures during the indentation process.

3 FEM and MD Analyses for the Indentation of Gold Particle

First, FEM and MD analyses are carried out to understand the process for two regimes in the compressive experiment of particles. In regime I, the nucleation of the very first dislocation plays a decisive role, while in regime II, the internal dislocation multiplication and propagation is conclusive. To distinguish these two mechanisms, we term the first collapse process as “correlated emission mechanism” and the second one as “accumulated emission mechanism.” These two dominant mechanisms will be analyzed in this section.

3.1 FEM Simulations. Based on the analysis of two different regimes above, we can assume that for regime I, the material is elastic before collapse since few dislocations nucleate at this period, and for regime II, an ideally elastic–plastic model is adopted because of the abundant internal dislocation multiplication. According to this, we carry out simple FEM simulations by commercial software ABAQUS for gold particle of diameter 500 nm using different material models to further confirm the assumptions above. In the FEM calculations, Young's modulus is 54 GPa and

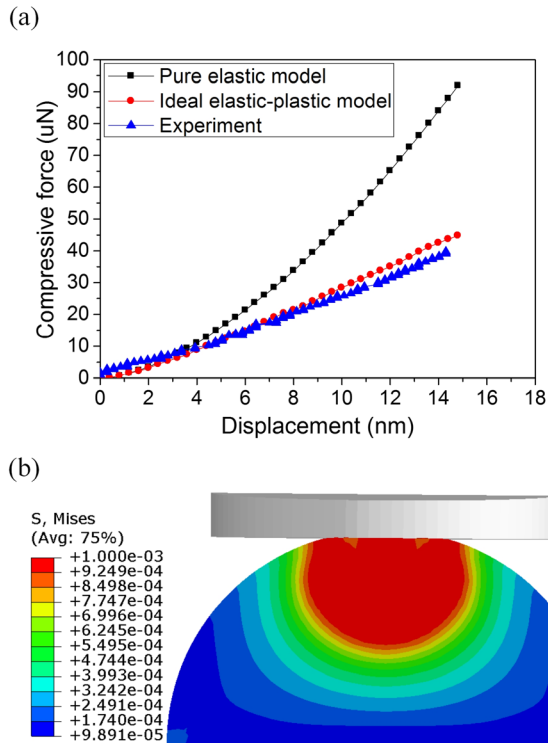


Fig. 3 (a) Compressive force versus displacement results of two simulations and experiment in 500 nm diameter particle; (b) Mises stress distribution in 500 nm diameter particle for ideally elastic-plastic model

Poisson's ratio is 0.4. Both elastic and ideally elastic-plastic models are adopted to verify the characteristic of the force-displacement curve. For the ideally elastic-plastic model, the peak stress at the onset of plasticity is chosen as 1.0 GPa, which falls in the range of 0.8–2.7 GPa reported for the theoretical strength of Au in various theoretical and numerical models [29–32]. In the simulations, the crystalline gold particle was divided into 31,824 C3D8 elements and the flat punch was simulated as a rigid body controlled by displacement loading as shown in Fig. 3. The simulation results in comparison with experimental data are given in Fig. 3(a). The results reveal that the load in the perfectly elastic type would rise in a parabola-kind way for the compressive experiment of the hemisphere-shaped samples. While for the ideally elastic-plastic model, the load increases in a linear way, and there is a significant high stress region just below the flat punch as shown in Fig. 3(b). Then, by comparing the FEM calculation results with experiment data in Fig. 2, we can find that the basic characters of the experimental load-displacement curves of particles with diameter 400 nm and 500 nm show an excellent linear relation before collapse, and the experiment data of 500 nm diameter particle match well with the ideally elastic-plastic model in the FEM simulations. This demonstrates that abundant dislocations nucleation and storage exist inside the particle during the compression experiments. In contrast, the compressive force of 300 nm diameter particle continues to rise in a parabola-kind way before collapse, which is consistent with the elastic model. It indicates that few dislocations nucleate inside the smaller particles. These results to some extent support that the accumulated emission mechanism controls the collapse of relative larger particles and correlated emission mechanism is dominant for the smaller ones.

3.2 MD Simulation. MD simulations are further carried out by using the large-scale atomic/molecular massively parallel simulator [33] within the framework of embedded atomic potential [34] to investigate the dislocation nucleation and propagation

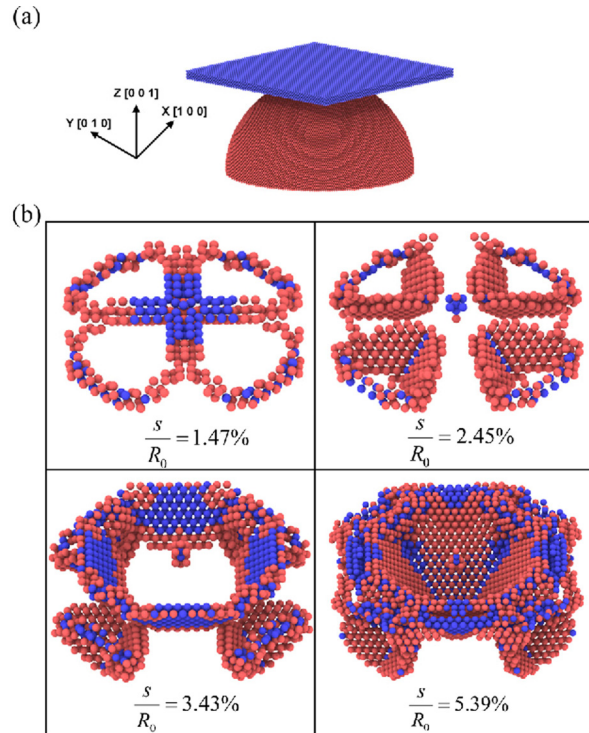


Fig. 4 (a) MD model of gold hemisphere particle compression; (b) dislocation structures under different compressive displacement and radius ratio, blue atoms with CSD > 7 while red atoms with CSD from 3 to 7

process in the gold particles. Although the maximum scale of particles which can be effectively handled by MD calculation is much smaller than the size tested in the experiment, and the loading rate is also much faster, MD simulation still serves as a widely accepted method to reveal the deformation details in small-scale materials.

The compressive model of gold hemisphere is setup without any defects under a nonperiodic boundary condition as shown in Fig. 4(a). A hemisphere-shaped particle with diameter 24.48 nm is established as the red atoms, and a diamond flat punch is denoted as the blue ones. Under the particle, there is a cylindrical base as high as 12.24 nm, which is not shown here. The diamond flat punch pushes down along with the direction [0 0 -1] while the bottom of the model is fixed. Here, we use the centrosymmetry deviation (CSD) parameter to indicate the location of defects in the particle. The dislocation structures and distribution under the indenter corresponding to different compressive displacements (normalized by the radius of hemisphere ratio) are given in Fig. 4(b).

The MD simulation results manifest that the dislocations prefer to nucleate closed to a flat punch because of the high stress at this region. The arc-shaped dislocations are formed at the four different slip planes and then pile up in a low stress area. This result also matches well with the anticipation of FEM simulation in Fig. 3(b). There is a localized stress concentration site just below the flat punch where the dislocation nucleation events would happen, and dislocation pile-ups also occurred due to the great change of stress level along with the distance far away from the contact point. So, it is possible that the release of numerous pile-up dislocation loops lead to the particle collapse.

4 Theoretical Model for the Indentation of Large Gold Sphere

Through comprehensive experimental observations and the numerical analyses in Secs. 2 and 3, it is clear that in case the

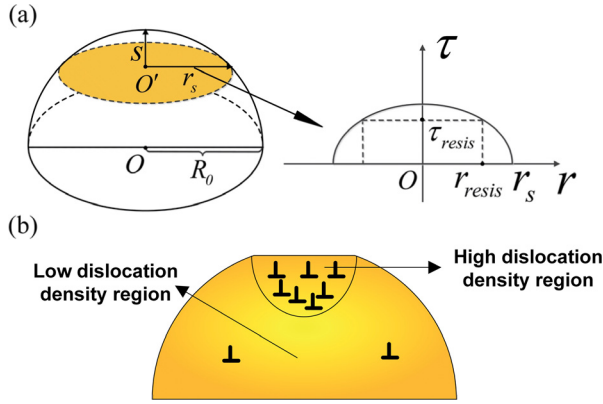


Fig. 5 (a) Shear stress distribution along the radius in a section plane of the hemisphere; (b) two regions divided by dislocation densities

so-called correlated emission mechanism control the collapse, the burst contact pressure at collapse point would be simply controlled by the surface nucleation stress. This case is suitable for the samples with small size, because dislocations are more probable to glide out instead of forming stable tangle within the particle. However, for bigger particles with diameter 400 nm and above, dislocations may accumulate inside, and it is difficult to estimate the critical point and understand the dislocation release process. Next, based on the experimental and numerical results above, we mainly focus on revealing the physical mechanism for the second type of collapse. A theoretical model is developed firstly to describe the dislocation density evolution and the energy conversion before the structural collapse. Then, a dislocation pile-up model is proposed to be responsible for the displacement burst, and some decisive factors are proposed for the collapse of spherical component at submicron scales.

4.1 Theoretical Model Before Collapse. Before the collapse of gold particles, a large-scale plasticity accompanied with multiple dislocation events occurred at the region below the indenter. During this process, the external work would be converted to various energy components.

4.1.1 Energy Balance Analysis. Along with the diamond flat punch compressing the specimen, the dislocations will soon nucleate near the contact surface of hemisphere because of the extremely high contact stress at this area. According to the numerical simulation results in Fig. 3, the Mises stress in an ellipsoidal region is high and there is a distinct stress gradient around the contact surface. As shown schematically in Fig. 5(a), the nonuniform distribution of shear stress along the radius at a cross section leads to the resolved shear stress near the lateral surface is smaller than the slip resistance τ_{resis} (corresponding to the radius r_{resis}), which results in the dislocations nucleation and pile up in the central part as shown in Fig. 4. According to both FEM and MD calculation results, the single crystalline gold hemisphere under an indenter can be divided into two characteristic regions for the simplicity of analytical analysis: high and low dislocation density regions, respectively, as shown in Fig. 5(b). The high density region is mainly considered to lead to the collapse.

During the compression process, from the viewpoint of energy conversion, the external work produced by diamond flat punch is converted to several energy components: An amount of dislocation nucleation energy due to the dislocation nucleation just below the flat punch, surface energy due to new surface creation and strain energy due to distortion deformation associated with the formation of dislocations, respectively.

Before the collapse occurs, for each small displacement increment δ , the external work for this increment can be expressed as

$$\Delta W = F \cdot \delta \quad (1)$$

This external work increment will be balanced by the increase of internal energy, which is mainly the dissipated energy and elastic energy associated with the newly nucleated arc-shaped dislocations as shown in Fig. 4(b). For simplicity, the arc-shaped dislocations located at the four slip planes can be regarded as a whole dislocation loop when calculating the total length of dislocations. Since the contact stress is high enough at the initial stage, it is reasonable to assume the size of newly formed dislocation loop is decided by the dimension of contact surface instead of the stress. So, the radius of newly nucleated dislocation loop can be expressed as ζr_s when the flat punch pushed down a length of burgers vector b . Here, r_s is the radius of contact surface as denoted in Fig. 5(a), and ζ is a proportional coefficient representing the ratio between the perimeter of the newly formed dislocation loop and contact surface.

For a group of dislocations in the high density region, the energy dissipated for the nucleation of original dislocations in each small displacement increment δ can be expressed in the following way [35]:

$$E_p = \tau b \cdot \zeta 2\pi r_s \cdot \zeta r_s \cdot \frac{\delta}{b} \quad (2)$$

where τ is the local shear stress, and ζ is the proportional coefficient mentioned above. Four items on the right side represent force per unit length, average length of newly formed dislocations, the average distance moved, and the number moved, respectively. The τ is chosen as two-thirds the compressive flow stress σ_f . Using s denotes the total compression displacement of particle and R_0 is the radius of gold hemisphere as shown in Fig. 5(a), the radius of the contact surface can be expressed as $r_s = \sqrt{2R_0s - s^2} \approx \sqrt{2R_0s}$ considering $s \ll R_0$.

Besides the dissipated dislocation nucleation energy, some other energies are stored within the distortion field around the created dislocation loops. Obviously, there are an amount of deformation energy stored in the high dislocation density region due to the distortion deformation around the dislocation loop itself, which is also a considerable strain energy stored in the whole particle. The total strain energy per unit length of a mixed dislocation loop is given by

$$E_d = \frac{Gb^2}{4\pi(1-\nu)} \ln \frac{R}{r} (1 - \nu \cos^2 \theta) + \frac{Gb^2}{10} \quad (3)$$

where R is an outer radius, choosing $R \approx r_s$, the dislocation core radius $r = b$. For a dislocation loop with half screw and half edge character, $\theta = \pi/4$. G is the shear modulus and ν is Poisson's ratio.

Then, the strain energy of the newly created dislocation loops during the displacement increment is given by

$$E_D = 2\zeta \pi r_s \cdot \frac{\delta}{b} \cdot E_d \quad (4)$$

And likewise, three items on the right side represent total length of a dislocation loop, numbers of newly nucleated loops, and strain energy per unit length, respectively.

At the same time, the external energy can also be expended for the new surface creation under the punch. This surface energy is taken into account as

$$E_S = \gamma_s \cdot \alpha \pi (r_{s+\delta}^2 - r_s^2) = 2\alpha \pi \gamma_s R_0 \delta \quad (5)$$

Here, γ_s is the surface energy per unit area and $\alpha \approx 1$ since the only contact surface is considered as the newly formed surface during the gold hemisphere compression test.

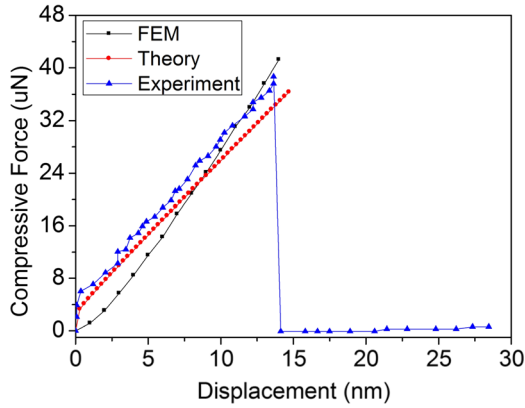


Fig. 6 The theoretical load–displacement curve is compared with the experiment data and FEM result of the particle with diameter 500 nm

The three kinds of internal energy discussed above are balanced by the external work. Based on the virtual work principle, the energy conservation equation can be expressed as

$$F \cdot \delta = \tau b \cdot 2\xi\pi r_s \cdot \xi r_s \cdot \frac{\delta}{b} + 2\xi\pi r_s \cdot \frac{\delta}{b} \cdot E_d + 2\alpha\pi\gamma_s R_0 \delta \quad (6)$$

Since Eq. (6) holds for any displacement increment δ , the external force F can be obtained by choosing $\tau = 2/3\sigma_f$

$$F = \frac{2}{3}\sigma_f b \cdot 2\xi\pi r_s \cdot \xi r_s \cdot \frac{1}{b} + 2\xi\pi r_s \cdot \frac{1}{b} \cdot E_d + 2\alpha\pi\gamma_s R_0 \quad (7)$$

There are several undetermined parameters, e.g., ξ , σ_f in this formulation, which will be decided, respectively, in the following analysis according to the experimental results for $D = 500$ nm.

4.1.2 Determination of Parameters. The proportional coefficient ξ will be decided by evaluating the dislocation density in high density region. At the initial stage of displacement, the contact area is very small and can provide large enough shear stress to nucleate and expand dislocation loops. Thus, we assume that a new dislocation loop is formed when the compressive displacement increases a characteristic length scale l , which is equal to $1/\sqrt{\rho}$. Here, we take the partial dislocations on four different planes as a perfect dislocation loop, and the total length of the newly nucleated dislocations in each small displacement increment is proportional to the perimeter of contact surface. These simplifications rely on the fact that the peak stress locates just below the flat punch and the nucleation of new dislocations is mainly influenced by the contact dimension instead of the stress state. Hence, the local dislocation density evolution equation can be given by

$$\frac{d\rho}{\sqrt{\rho}} = \frac{2\xi\pi r_s}{\frac{2}{3}\pi r_s^3} \cdot ds \quad (8)$$

where ξ is the proportional coefficient, and r_s is the radius of the contact surface as mentioned previously.

Given the initial condition that the radius of the first nucleated dislocation loop is equal to the length of burgers vector $b = 0.286$ nm, and the final condition is that $\rho = 1.18 \times 10^{15}/\text{m}^2$ while $s \approx 13 \times 10^{-9}$ m at collapse point observed in the test of 500 nm particles, $\xi = 1$ is obtained by solving Eq. (8). This indicates that for each displacement increment l , nearly one dislocation loop with radius equal to the radius of contact surface forms and this is consistent with the dislocation structure in our MD simulations. Through the integral of Eq. (8), the local dislocation

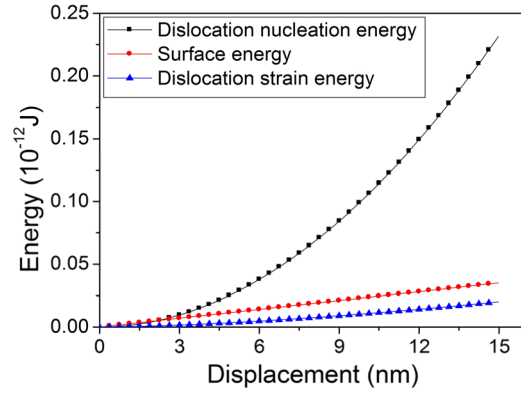


Fig. 7 Three distinct energy forms versus displacement from theoretical model

density in high dislocation density region then evolves in the following way:

$$\rho = \left(\frac{3}{4R_0} \cdot \ln \frac{s}{s_0} \right)^2 \quad (9)$$

where $s_0 = b^2/2R_0$ is an initial displacement corresponding to the formation of the first dislocation loop or four arc-shaped dislocations.

The Young's modulus is 54 GPa, and Poisson's ratio is 0.4 for Au, which are the same material constants as in FEM simulation. The surface energy per unit area γ_s for Au is 1.49 J/m^2 . Besides, for the gold particle with diameter of 500 nm, compressive flow stress σ_f is 1.0 GPa, which is the same value as in the ideally elastic–plastic model of FEM simulation.

4.1.3 Comparison With Experimental Data. From all the analyses above, the theoretical load–displacement curve is obtained as shown in Fig. 6, which is compared with the experiment data and FEM result of the particle with diameter 500 nm.

For the stage before collapse, the analytical results of external force agree well with the experiment data and FEM simulation results as shown in Fig. 6. It can be seen that the theoretical load is slightly smaller than the experiment data. This may be due to the neglect of the elastic strain energy in the low dislocation density region. At the initial stage, the load increases stably without evident bursts with the advance of displacement. This is because that the dislocation loops can continuously nucleate and store inside the particles. The nucleation of dislocation loops at subcritical size may lead to instability. However, the high stress zone in the particles is quite small compared to the whole sample, so the dislocations could be suppressed in a certain zone such as the high dislocation density region. Thus, the sudden bursts of deformation could not be induced for the moment.

Through integrating each item on the right side of Eq. (7), each energy component before collapse is plotted in Fig. 7. Obviously, a considerable part of the external work is converted into the dislocation nucleation energy. The strain energy stored in the dislocation is especially smaller compared with the other two parts. However, it is reasonable that the high density region is quite small and much more energy is required to create new dislocation loops instead of to deform field around the dislocation. The emission of these dislocations would lead to the irreversible plasticity instability.

From Eq. (7), the contact pressure before the collapse point can be calculated as

$$\sigma_p = \frac{F}{\pi r_s^2} = \frac{F}{2\pi R_0 s} = \frac{4}{3}\xi^2 \sigma_f + \frac{\sqrt{2}\xi}{b\sqrt{R_0 s}} \cdot E_d(s) + \frac{\alpha\gamma_s}{s} \quad (10)$$

So, the theoretical contact pressure at the dislocation nucleation dominated stage is mainly affected by the specimen size R_0 , compression displacement s , and compressive flow stress σ_f ,

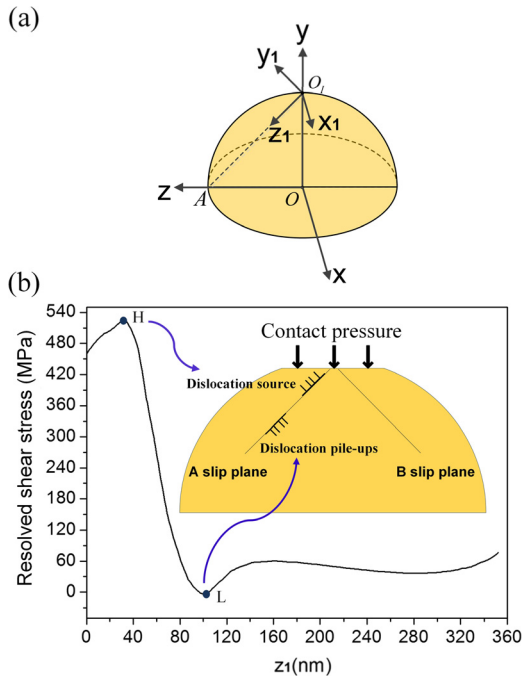


Fig. 8 (a) Two coordinate systems in a gold hemisphere. (b) Local resolved shear stress distribution along O_1A .

respectively. Moreover, if assuming the critical compressive displacement at the collapse point is s_c , then the critical contact pressure can be expressed as

$$\sigma_{pc} = \left(\frac{4}{3} \zeta^2 \sigma_f + \frac{\alpha \gamma_s}{s_c} \right) + \frac{1}{\sqrt{R_0}} \cdot \frac{\sqrt{2} \zeta E_d(s_c)}{b \sqrt{s_c}} \quad (11)$$

Here, a size dependent critical contact pressure is obtained from Eq. (11). On the right side of Eq. (11), the first item $4/3 \zeta^2 \sigma_f$ in the bracket, related to the internal dislocation nucleation process, is relatively larger than the second item by comparing the dislocation nucleation energy with surface energy. Therefore, at this stage, it is a dislocation nucleation and storage dominant process. The external force is mainly balanced by the internal energy from this process. For the particle with diameter 500 nm, the burst displacement s_c is around 13 nm. By substituting this value into Eq. (11), we can get the critical contact pressure is 1526 MPa, which is close to the experiment value 1481 MPa. It should be noted that the critical contact pressure for much smaller samples is not able to be obtained accurately from Eq. (11), since this result is on the base of dislocation accumulation process and this mechanism is not dominant for small particles. Afterwards, this accumulation of numerous dislocations would become unstable with the punch continuously pushing down. A further interpretation for how these dislocations pile up and induce the instability would be discussed in Sec. 4.2.

4.2 Theoretical Analysis of the Collapse. For the accumulated emission mechanism, the dislocation storage and emission configuration inside the gold hemisphere is discussed in this section. The local shear stress along a typical slip direction is analyzed and the dislocation distribution is also calculated through the force balance of a dislocation.

4.2.1 Local Resolved Shear Stress Distribution. From the experimental observations, the hemispherical particles are almost defect-free after collapse. It means that most dislocations move out of the specimen simultaneously when the collapse happens. So what breaks the equilibrium of dislocations at the collapse

point? In the following, the emissions of multiple dislocation loops are proposed to illustrate the particle collapse process.

As observed in the MD simulations, numerous dislocations nucleate on different slip planes in the gold particles before collapse. The massive dislocations stored in the high dislocation density region are in a static equilibrium state under the long- and short-range interactions between dislocations, which can be regarded as an equilibrium “multibody system” to some extent. As the increase of new dislocations, this region could not afford more dislocations. The equilibrium state will be broken and some dislocations will run out to decrease the free energy of the system. The primitive emission will simultaneously cause the emissions of massive dislocations in the high density region. This kind of perturbation around an emitted dislocation releases the internal energy to activate and drive numerous dislocations to move progressively. A plenty of dislocation emissions driven by the energy stored in the material will cause irreversible damage to the structure configuration and lead to the particle collapse phenomenon. So, whether the collapse could happen depends on the degree of dislocation accumulations inside the particle and the activation of dislocation emissions from the free surface. The dislocation accumulation is the preparatory condition for the emissions of collective dislocation loops or arc-shaped dislocations. This is also why the dislocation nucleation energy is much larger than the other two energy components before collapse as plotted in Fig. 7.

In order to give a further illustration for this dislocation accumulation process, a local resolved shear stress $\tau_r = n \cdot \sigma \cdot s$ distribution along a dislocation slip direction is given in Fig. 8. Here, n is a unit normal to the slip plane and s is a unit vector along the glide direction. For the gold particles, a global coordinate system “ $O-xyz$ ” and a local coordinate system “ $O_1-x_1y_1z_1$ ” on a slip direction are established as shown in Fig. 8(a), where z_1 is along the slip direction and $x_1O_1z_1$ is the slip plane. The local resolved shear stress distribution along O_1A (A is the intersection point of z_1 with z) in a particle with diameter 500 nm is plotted in Fig. 8(b) for the compression displacement $s = 9$ nm. It is clear that a great stress gradient exists since the stress decreases rapidly with the increase of the distance away from point O_1 . The peak shear stress at point “ H ” locates at a short distance away from the contact surface. This is why we observed that the site of dislocation nucleation was a little far away from the indenter in the experiments and simulations. Besides, when the distance to O_1 reaches some value, a stress valley region appears where the local shear stress can decline to zero and even reverse at point “ L ” as shown in Fig. 8(b). It is worth mentioning that the stress distributions are similar in particles with different sizes under different compressive displacements, while the locations of the stress valley region may change a little. Dislocations would pile up at this stress valley region along with the slip plane.

4.2.2 Pile-Up Model. In this section, the distribution of dislocations along a typical slip direction is given quantitatively. As the resolved shear stress is in a linear distribution between the stress peak and valley, respectively, the schematic of stress distribution is shown in Fig. 9(a). The stress along the slip direction $[0 - 1]$ can be expressed as

$$\tau(z) = \tau_0 - \frac{z}{L} \cdot \tau_0 \quad (12)$$

where τ_0 is the peak stress and L is the distance between stress peak and stress valley.

Under the condition of a linear stress distribution, the interaction of the dislocation at position z with all the other dislocations at position z' must balance the local resolved shear stress $\tau(z)$. Thus, the Peach–Koehler force balance is [36]

$$\tau(z)b = \frac{Gb^2}{2(1-\nu)} \int_0^L \frac{n(z')}{z' - z} dz', \quad 0 \leq z \leq L \quad (13)$$

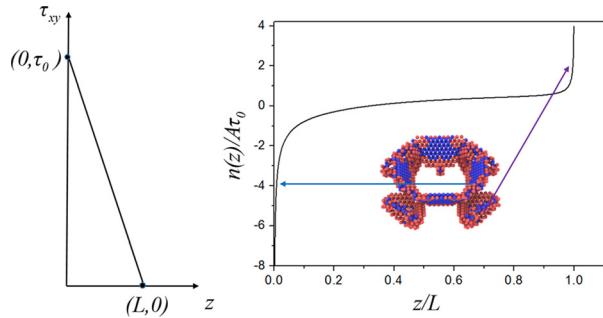


Fig. 9 (a) Linear stress distribution along a slip direction. (b) Plot of the normalized dislocation distribution as a function of location.

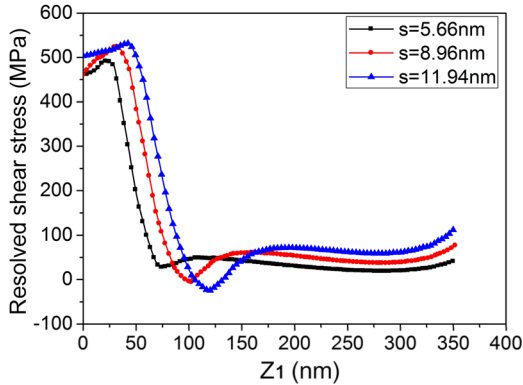


Fig. 10 Stress distribution along the slip direction under different compressive displacement in sample with diameter 500 nm

Here, $n(z) = (db/dz)/b$ is the dislocation density, i.e., the number of dislocations between z and $z + dz$.

Through integrating the equation on the right by the Hilbert transform and a coordinate transformation, we can get the dislocation along a slip direction as

$$\frac{n(z)}{A\tau_0} = \frac{1}{2} \cdot \frac{3z - \frac{3}{4}L - 2\frac{z^2}{L}}{\sqrt{Lz - z^2}} \quad (14)$$

where the coefficient A is

$$A = \frac{2(1-\nu)}{Gb} \quad (15)$$

This dislocation density distribution is plotted in Fig. 9(b). The positive or negative sign of $n(z)$ represents different direction of burgers vector. This distribution matches well with the qualitative analysis previously. Abundant dislocations would be accumulated in two typical areas. The stress peak zone is the source where dislocations form, while the stress valley area is the location for dislocation pile-ups. However, it is worth mentioning that the stress valley still locates some distance away from the lateral free surface. This dislocation distribution provides a clear evidence for the pile-up configuration.

Returning to Eq. (14), the distance L between stress peak and valley depends on the particle size R . However, for the specimen with a specific size, it seems that this distance does not change during the flat punch pushing down and the stress peak and valley areas would shift integrally as shown in Fig. 10. Meanwhile, more dislocations nucleate as the peak stress increases. Thus, once the stress valley area or the dislocation pile-up zone gets close to the lateral surface, dislocations will become unstable under the attraction of the free surface.

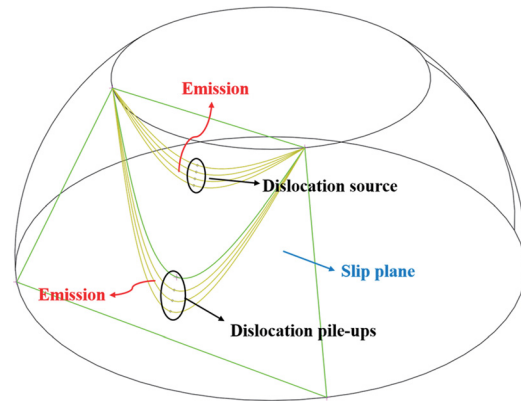


Fig. 11 Configuration of dislocations on a slip plane and the emission process at critical state at the collapse point

By this moment, a scene for dislocation emission process can be plotted out. The gold particle system is able to stay in a static equilibrium state before collapse. As the flat punch pushes down, dislocations would nucleate in the stress peak region. The schematic diagram of a typical dislocation emission process is shown in Fig. 11. Before the collapse point, the dislocation loops on a slip plane pile up at two typical zones: one is the stress peak area for dislocation nucleation and the other one is the stress valley zone where dislocations pile up. As shown in Figs. 10 and 11, these two zones would shift to be closer to the lateral surface along with the punch pushing down. At some critical point, the image force from the free surface will break the dislocation pile-ups and drive the unstable dislocations in the stress valley zone to escape from the lateral surface. Once this emission condition is reached, the original equilibrium state will be broken. These incipient dislocation emissions would lead to the initial slight collapse. Since the slip velocity of a dislocation is much faster than the loading speed of punch, the punch could not follow the deformation of the particle collapse. Thus, the punch keeps some distances away from the particle, which leaves another free surface on the top of hemisphere. The dislocations at this region are also activated and emitted. Dislocation avalanches arise from the release of these pile-ups lead to the sudden collapse, and the hemisphere-shaped particle deforms as frustum of a cone without dislocations.

In this model, once a dislocation nucleates at the site of stress peak, it will soon expand spontaneously to the stress valley zone due to the stress gradient along the same slip plane. The length of this journey just depends on the sample size and the compressive displacement shifts the stress peak and valley integrally to be closer to the lateral free surface. More generally, the dislocation nucleation and accumulation processes depend not only on the peak stress but also on the stress gradient. This explains why large displacement bursts are also observed in the compression of pillars with oxide layer, which corresponds to the sudden emission of pile-ups at the interface. In addition to the barriers, the dislocation pile-ups can also be caused by the stress valley in an inhomogeneous stress field. The collapse will bring some troubles to the fabrication of devices at submicron scales.

5 Conclusions

In this paper, one kind of sensitive material behavior is observed in the compression experiment of single crystalline gold particles with diameter ranging from 300 to 700 nm embedded a half in a silicon substrate. The particle suddenly collapses and numerous dislocations escape from the free surface during a flat punch moving toward the particle. Two kinds of dominant mechanisms are proposed to explain the particle collapse at submicron scale, which are the correlated emission mechanism for small-size samples and the accumulated emission mechanism for large ones.

For the particle with smaller size, the correlated emission mechanism is responsible due to the significant effect of lateral surface and the convenience to achieve a clean surface. The collapse would simply depend on the onset of the first dislocation nucleation event. While for the particle with larger size, the dislocation nucleation and accumulation are dominant. Both FEM and MD simulations show that dislocation accumulation occurs at the stress concentration sites close to the flat punch. The FEM calculations provide a straight comparison for the two proposed mechanisms. Dislocation avalanches arise from the release of dislocation pile-ups in the stress valley zone.

Theoretical analysis is focused on the large samples. Two characteristic regions divided by the dislocation density are proposed due to the stress distribution in FEM analysis and the dislocation structures in MD simulation. A theoretical model is developed, and the dislocation nucleation and evolution are investigated. The analytical solution is deduced based on the principle of virtual work. For the stage before collapse, the analytical results of compressive force balanced by the dislocation-based internal energy agree well with the experiment data. A large number of dislocations can nucleate in the stress peak zone and pile up at stress valley on a slip plane. The dislocation nucleation and accumulation processes depend not only on the peak stress near the vertices but also on the stress gradients along the slip plane. The progressive dislocation emissions at the pile-up zone result in a large-scale collapse and cause an irreversible damage, as well as release large elastic deformation around the pile-up dislocations at the two typical zones.

Acknowledgment

This work was supported by the Key Program of National Natural Science Foundation of China (NSFC) through Grant Nos. 11132006 and 11302115, National Key Fundamental Research Grant (973) No. 2010CB631005.

References

- [1] Greer, J. R., and De Hosson, J. T. M., 2011, "Plasticity in Small-Sized Metallic Systems: Intrinsic Versus Extrinsic Size Effect," *Prog. Mater. Sci.*, **56**(6), pp. 654–724.
- [2] Kim, J.-Y., Jang, D., and Greer, J. R., 2012, "Crystallographic Orientation and Size Dependence of Tension–Compression Asymmetry in Molybdenum Nanopillars," *Int. J. Plast.*, **28**(1), pp. 46–52.
- [3] Gu, R., and Ngan, A. H. W., 2013, "Dislocation Arrangement in Small Crystal Volumes Determines Power-Law Size Dependence of Yield Strength," *J. Mech. Phys. Solids*, **61**(6), pp. 1531–1542.
- [4] Greer, J. R., Oliver, W. C., and Nix, W. D., 2005, "Size Dependence of Mechanical Properties of Gold at the Micron Scale in the Absence of Strain Gradients," *Acta Mater.*, **53**(6), pp. 1821–1830.
- [5] Heyer, J. K., Brinckmann, S., Pfetzinger-Micklich, J., and Eggeler, G., 2014, "Microshear Deformation of Gold Single Crystals," *Acta Mater.*, **62**, pp. 225–238.
- [6] Argon, A. S., 2013, "Strain Avalanches in Plasticity," *Philos. Mag.*, **93**(28–30), pp. 3795–3808.
- [7] Wang, Z.-J., Li, Q.-J., Shan, Z.-W., Li, J., Sun, J., and Ma, E., 2012, "Sample Size Effects on the Large Strain Bursts in Submicron Aluminum Pillars," *Appl. Phys. Lett.*, **100**(7), p. 071906.
- [8] Gu, R., and Ngan, A. H. W., 2012, "Effects of Pre-Straining and Coating on Plastic Deformation of Aluminum Micropillars," *Acta Mater.*, **60**(17), pp. 6102–6111.
- [9] Kiener, D., Hosemann, P., Maloy, S. A., and Minor, A. M., 2011, "In Situ Nanocompression Testing of Irradiated Copper," *Nature Mater.*, **10**(8), pp. 608–613.
- [10] Zaiser, M., Schwerdtfeger, J., Schneider, A. S., Frick, C. P., Clark, B. G., Gruber, P. A., and Arzt, E., 2008, "Strain Bursts in Plastically Deforming Molybdenum Micro- and Nanopillars," *Philos. Mag.*, **88**(30–32), pp. 3861–3874.
- [11] Suresh, S., Nieh, T.-G., and Choi, B. W., 1999, "Nano-Indentation of Copper Thin Films on Silicon Substrates," *Scr. Mater.*, **41**(9), pp. 951–957.
- [12] Gouldstone, A., Kon, H.-J., Zeng, K.-Y., Giannakopoulos, A. E., and Suresh, S., 2000, "Discrete and Continuous Deformation During Nanoindentation of Thin Films," *Acta Mater.*, **48**(9), pp. 2277–2295.
- [13] Uchic, M. D., Dimiduk, D. M., Florando, J. N., and Nix, W. D., 2004, "Sample Dimensions Influence Strength and Crystal Plasticity," *Science*, **305**(5686), pp. 986–989.
- [14] Nix, W. D., Greer, J. R., Feng, G., and Lilleodden, E. T., 2007, "Deformation at the Nanometer and Micrometer Length Scales: Effects of Strain Gradients and Dislocation Starvation," *Thin Solid Films*, **515**(6), pp. 3152–3157.
- [15] Csikor, F. F., Motz, C., Weygand, D., Zaiser, M., and Zapperi, S., 2007, "Dislocation Avalanches, Strain Bursts, and the Problem of Plastic Forming at the Micrometer Scale," *Science*, **318**(5848), pp. 251–254.
- [16] Li, H., Ngan, A. H. W., and Wang, M. G., 2011, "Continuous Strain Bursts in Crystalline and Amorphous Metals During Plastic Deformation by Nanoindentation," *J. Mater. Res.*, **20**(11), pp. 3072–3081.
- [17] Zhou, C., Biner, S., and Lesar, R., 2010, "Simulations of the Effect of Surface Coatings on Plasticity at Small Scales," *Scr. Mater.*, **63**(11), pp. 1096–1099.
- [18] Ispánovity, P. D., Groma, I., Györgyi, G., Csikor, F. F., and Weygand, D., 2010, "Submicron Plasticity: Yield Stress, Dislocation Avalanches, and Velocity Distribution," *Phys. Rev. Lett.*, **105**(8), p. 085503.
- [19] Gerberich, W. W., Mook, W. M., Chambers, M. D., Cordill, M. J., Perrey, C. R., Carter, C. B., Miller, R. E., Curtin, W. A., Mukherjee, R., and Girshick, S. L., 2006, "An Energy Balance Criterion for Nanoindentation-Induced Single and Multiple Dislocation Events," *ASME J. Appl. Mech.*, **73**(2), pp. 327–334.
- [20] Li, J., Vliet, K. J. V., Zhu, T., Yip, S., and Suresh, S., 2002, "Atomistic Mechanisms Governing Elastic Limit and Incipient Plasticity in Crystals," *Nature*, **418**(18), pp. 307–310.
- [21] Tsuru, T., Shibutani, Y., and Kaji, Y., 2010, "Nanoscale Contact Plasticity of Crystalline Metal: Experiment and Analytical Investigation Via Atomistic and Discrete Dislocation Models," *Acta Mater.*, **58**(8), pp. 3096–3102.
- [22] Van Vliet, K., Li, J., Zhu, T., Yip, S., and Suresh, S., 2003, "Quantifying the Early Stages of Plasticity Through Nanoscale Experiments and Simulations," *Phys. Rev. B*, **67**(10), p. 104105.
- [23] Xu, S., Guo, Y. F., and Ngan, A. H. W., 2013, "A Molecular Dynamics Study on the Orientation, Size, and Dislocation Confinement Effects on the Plastic Deformation of Al Nanopillars," *Int. J. Plast.*, **43**, pp. 116–127.
- [24] Weinberger, C. R., and Cai, W., 2010, "Plasticity of Metal Wires in Torsion: Molecular Dynamics and Dislocation Dynamics Simulations," *J. Mech. Phys. Solids*, **58**(7), pp. 1011–1025.
- [25] Ng, K. S., and Ngan, A. H. W., 2008, "A Monte Carlo Model for the Intermittent Plasticity of Micro-Pillars," *Modell. Simul. Mater. Sci. Eng.*, **16**(5), p. 055004.
- [26] Li, S., Ren, B., and Minaki, H., 2014, "Multiscale Crystal Defect Dynamics: A Dual-Lattice Process Zone Model," *Philos. Mag.*, **94**(13), pp. 1414–1450.
- [27] Cui, Y. N., Lin, P., Liu, Z. L., and Zhuang, Z., 2014, "Theoretical and Numerical Investigations of Single Arm Dislocation Source Controlled Plastic Flow in FCC Micropillars," *Int. J. Plast.*, **55**, pp. 279–292.
- [28] Wang, Z.-J., Shan, Z.-W., Li, J., Sun, J., and Ma, E., 2012, "Pristine-to-Pristine Regime of Plastic Deformation in Submicron-Sized Single Crystal Gold Particles," *Acta Mater.*, **60**(3), pp. 1368–1377.
- [29] Chuang Deng, F. S., 2009, "Near-Ideal Strength in Gold Nanowires Achieved Through Microstructural Design," *ACS Nano*, **3**(10), pp. 3001–3008.
- [30] Ogata, S., Li, J., Hirosaki, N., Shibutani, Y., and Yip, S., 2004, "Ideal Shear Strain of Metals and Ceramics," *Phys. Rev. B*, **70**(10), p. 104104.
- [31] Gall, K., Diao, J., and Dunn, M. L., 2004, "The Strength of Gold Nanowires," *Nano Lett.*, **4**(12), pp. 2431–2436.
- [32] Volkert, C. A., and Lilleodden, E. T., 2006, "Size Effects in the Deformation of Sub-Micron Au Columns," *Philos. Mag.*, **86**(33–35), pp. 5567–5579.
- [33] Plimpton, S., 1995, "Fast Parallel Algorithms for Short-Range Molecular Dynamics," *J. Comput. Phys.*, **117**(1), pp. 1–19.
- [34] Foiles, S., Baskes, M., and Daw, M., 1986, "Embedded-Atom-Method Functions for the FCC Metals Cu, Ag, Au, Ni, Pd, Pt, and Their Alloys," *Phys. Rev. B*, **33**(12), pp. 7983–7991.
- [35] Gerberich, W. W., 2006, "An Energy Balance Criterion for Nanoindentation-Induced Single and Multiple Dislocation Events," *ASME J. Appl. Mech.*, **73**(2), pp. 327–334.
- [36] Akarapu, S., and Hirth, J. P., 2013, "Dislocation Pile-Ups in Stress Gradients Revisited," *Acta Mater.*, **61**(10), pp. 3621–3629.